

# Development and application of a hybrid prestressed segmental concrete girder utilizing low carbon materials

Jun-Mo Yang<sup>1</sup> and Jin-Kook Kim\*<sup>2</sup>

<sup>1</sup>Department of Civil Engineering, Keimyung University, 1095 Dalgubeol-daero, Dalseo-gu, Daegu 42601, Republic of Korea

<sup>2</sup>Department of Civil Engineering, Seoul National University of Science and Technology, 232 Gongneung-ro, Nowon-gu, Seoul 01811, Republic of Korea

(Received November 26, 2018, Revised December 19, 2018, Accepted January 21, 2019)

**Abstract.** A hybrid prestressed segmental concrete (HPSC) girder utilizing low carbon materials was developed in this paper. This paper introduces the hybrid prestressing concept of pre-tensioning the center segment and assembling all segments by post-tensioning, as well as the development process of the low carbon HPSC girder. First, an optimized mix proportion of 60 MPa high strength concrete containing high volume blast furnace slag was developed, then its mechanical properties and durability characteristics were evaluated. Second, the mechanical properties of 2,400 MPa high strength prestressing strands and the transfer length characteristics in pre-tensioned prestressed concrete beams were evaluated. Third, using those low carbon materials and the hybrid prestressing concept, the HPSC girders were manufactured, and their structural performance was evaluated. A 30-m long HPSC girder for highway bridges and a 35-m long HPSC girder for railway bridges were designed, manufactured, and structurally confirmed as having sufficient strength and safety. Finally, five 35-m long HPSC girders were successfully applied to an actual railway bridge for the first time.

**Keywords:** HPSC girder; 2,400 MPa prestressing strand; low carbon concrete; blast furnace slag; field application

## 1. Introduction

Concrete girders are susceptible to cracking due to tensile stress, but an efficient cross section design for concrete is possible by introducing prestressing force through pre-tension or post-tension. Prestressed concrete (PSC) girders have recently been applied to 50-60-m long highway bridges and 35-40-m long railway bridges, thanks to improvements in the materials used and the construction method. Among PSC girders, the PSC-I girders occupy most PSC bridges due to their low construction cost, relatively simple construction, shorter period of construction, and the fact that they have been widely used for various road bridges and railway bridges (Hamilton and Brenkus 2013, Han *et al.* 2003).

In some developed countries, PSC-Box type and PSC-I type bridge girders have been manufactured in segments at factories and assembled on site through the prestressing of strands for several decades. In the United States, full-length pre-tensioned prestressed concrete girders are commonly used because long-span girders can be transported by land in many states. In a recent development (Hamilton *et al.* 2013), transportable segments were pretensioned at a precast yard, and the strands were cut prior to transport, then spliced on site. Prestressing force was applied to the system by hydraulic jacks on each side of the girder web. External brackets transferred the force from the hydraulic

jacks to the precast segments by thru-bolts that passed through the web of the beam. The internal restraint provided by the coupled prestressing strand resisted the jacking force, and the prestressing strand was stressed. In Korea, the PSC-I type segment bridge method has been partially developed and is gradually being expanded, however, pretensioned prestressed girders are rarely used due to their transportation limitations.

Interest in environmentally friendly concrete, which minimizes carbon dioxide emissions, has recently been increasing worldwide (Menendez *et al.* 2003, Mahmoud *et al.* 2013). The production of Portland cement contributes to a large portion of anthropogenic CO<sub>2</sub> emissions, thus, a key challenge is to reduce the amount of Portland cement used in concrete mixtures. Cementitious materials, such as fly ash and blast furnace slag (BFS), are widely used as substitutes for Portland cement because of their pozzolanic reactivity and latent hydraulic activity (Jeon *et al.* 2006). In addition, the concrete mixture substituted with such an admixture has excellent long-term strength and is widely used for high-strength concrete. This is because the sizes of the mineral particles are smaller than those of the Portland cement, so that a more compact structure can be achieved. This property can be effectively applied to a PSC structure requiring high compressive strength.

Other high-performance construction materials besides concrete can also be useful for reducing CO<sub>2</sub> emissions. One example is the recently developed 2,400 MPa high strength prestressing steel strand (Kim *et al.* 2013). By using the strand, which has a tensile strength that is increased by about 28% compared to that of the conventional prestressing strand, the prestressing tendons

---

\*Corresponding author  
E-mail: [jinkook.kim@seoultech.ac.kr](mailto:jinkook.kim@seoultech.ac.kr)

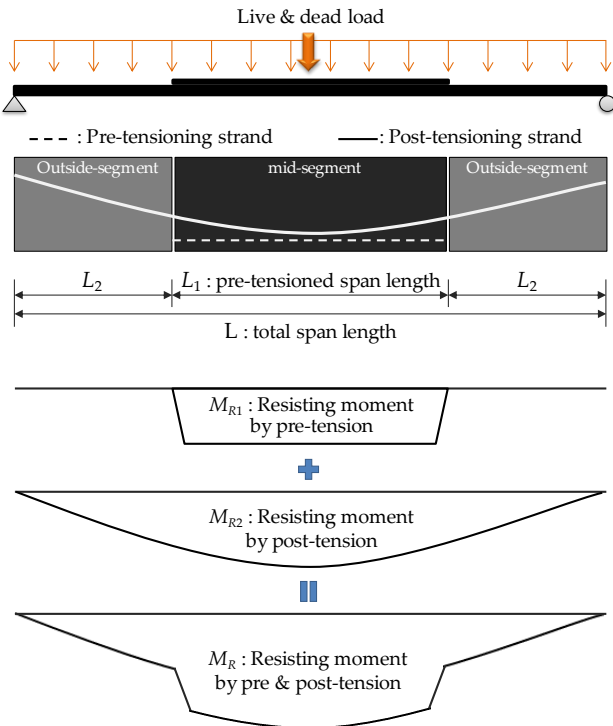


Fig. 1 Concept of HPSC girder

Table 1 Mix proportions

W/C (%)	BFS/B (%)	S/a (%)	$G_{max}$ (mm)	Unit weight (kg/m <sup>3</sup> )					AEWR (%)	
				W	C	BFS	S	G		
25.0,	0, 40,	41.1	20	163	163	0	628	882	0.6	
27.5,	50, 60,	~			~	~	~	~	~	~
30.0	70	43.7			652	456	721	932	0.8	

[Note] W/C = water-to-cement ratio, BFS/B = ratio between blast furnace slag and total binder (cement + blast furnace slag), S/a = weight ratio of sand to total aggregate,  $G_{max}$  = maximum size of gravel, W = water, C = cement, BFS = blast furnace slag, S = sand, G = gravel, AEWR = air-entraining and water-reducing agent.

and the cross-sectional area of the girder can be reduced, so that it can reduce the CO<sub>2</sub> emissions of the PSC girder in the fabrication stage.

In this paper, a newly developed hybrid prestressed segmental concrete (HPSC) girder, constructed by pre-tensioning the center segment in the factory and assembling all other segments through post-tensioning in the field, utilizing low carbon materials is introduced. Previously published papers (Kim *et al.* 2016, Yang *et al.* 2016, Yang *et al.* 2017, Yang *et al.* 2018, Yim *et al.* 2018) are summarized, new contents are added, and all those are organized systematically. First, the application basis for low carbon materials was established. The optimized mix proportion of 60 MPa high strength concrete containing high volume blast furnace slag, 60% replacement, was developed, and its mechanical properties and durability characteristics were evaluated. The mechanical properties of the 2,400 MPa high strength prestressing strand and the transfer length characteristics in the pre-tensioned prestressed concrete beams were evaluated. Afterward,

using those low carbon materials, the HPSC girders were manufactured and its structural performance was evaluated. Two full-scale bridge girders, a 30-m long HPSC girder for a highway bridge and a 35-m long HPSC girder for a railway bridge, were designed, manufactured, and tested by cyclic and static loads. Finally, the 35-m long HPSC girder was applied for the first time to an actual railway bridge at the Railroad Test Track in Sejong city, Korea.

## 2. Concept of hybrid prestressed segmental concrete girder

The concept of an HPSC girder is an efficient concept that combines the advantages of pre-tension and post-tension methods. A schematic that illustrates the segmental combination and prestressing process is presented in Fig. 1. The HPSC girder consists of a mid-segment and outside-segments. The mid-segment is fabricated through pre-tensioning, and each segment is pre-fabricated at the factory, then moved to the site after sufficient curing. This makes it possible to control cracks due to self-weight during transport, even if the mid-segment is made longer. The outside-segments to which the pre-tension force is not introduced and the mid-segment to which the pre-tension is introduced are assembled together by introducing post-tension force into the entire length. The post-tensioning amount of the outside-segment can be reduced by  $((M_{R1}) / (M_{R1} + M_{R2}))$ , because the pre-tension is introduced into the mid-segment in advance, where  $M_{R1}$  and  $M_{R2}$  are the resisting flexural moment by pre-tension and post-tension, respectively. If the pre-tensioned mid-segment can support 30% of the total moment, the amount of post-tension at the outside-segment will be reduced by about 30%. This also means that total amount of tendon can be reduced by  $(30\% \times 2 \times L_2 / L)$ . For example, if  $(L_1 = 1.5 \times L_2)$ , the total amount of tendon can be reduced by about 17%.

The HPSC girder has the following additional advantages: (1) The required internal structures for the PSC girder, such as sheath, anchorage, and anchorage zone reinforcement, can be decreased in size. (2) Through factory production of each segment, it is possible to secure a good quality of concrete, to make segments quickly, and to minimize the pre-tension loss due to shrinkage of concrete. (3) The site works such that the installation of tendons and post-tensioning can be reduced.

## 3. Properties of low carbon materials

### 3.1 Concrete

#### 3.1.1 Mix optimization of concrete

One of the main objectives of this study is to apply low carbon concrete to a PSC girder. Concrete technology, which uses industrial by-products as a cementitious material, is an eco-friendly technology that reduces cement usage and reduces CO<sub>2</sub> emissions, and has already become a commonly used technology that is utilized in actual structures. However, if the cement replacement ratio of the industrial by-products is high, the strength development of

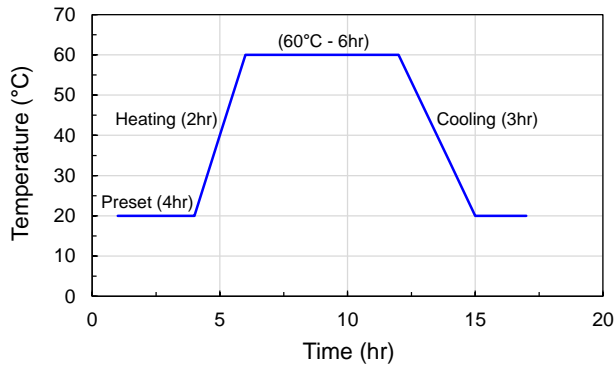


Fig. 2 Temperature history for steam curing (Yang *et al.* 2017)

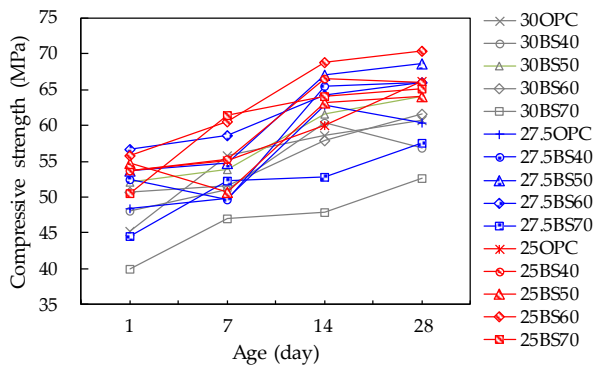


Fig. 3 Result of compressive strength test

the concrete at an early age is delayed, and this makes it difficult to utilize it in the PSC girder, which requires high strength of concrete at prestress release. This study has solved this problem by developing optimized mix proportions of concrete that can maximize concrete strength at early and long-term ages while increasing the replacement ratio of industrial by-products (Yang *et al.* 2017).

Blast furnace slag, which can maximize the industrial by-product replacement ratio, was selected as a cementitious material. With target compressive strengths of 48 MPa and 60 MPa at 1-day and 28-days, respectively, the effects of the water-to-binder (W/B) ratio and BFS replacement ratio upon concrete compressive strength were examined in order to determine the optimized mix proportions. Table 1 shows the concrete mix proportions used to obtain the optimized mixture proportions. Detailed mix proportions can also be found in Yang *et al.*'s paper (2017). Three different W/B ratios (25, 27.5, and 30%) and five different ratios of cement replacement by BFS (0, 40, 50, 60, and 70%) were tested. The unit water content was held constant at 163 kg/m<sup>3</sup>, and various fine aggregate ratios (S/a) from 41.1 to 43.7% were used. Type I Portland cement and Type III BFS were adopted as the cementitious materials. Crushed aggregate was adopted as the fine aggregate, and a coarse aggregate of maximum size 20 mm was also used. A polycarboxylic acid-based air-entraining and water-reducing admixture was incorporated in order to attain the required workability. The workability of concrete was controlled by 600 mm slump flow. Steam curing with heat was adopted in order to make precast prestressed

Table 2 Optimized mix proportions and mechanical properties

W/C (%)	BFS/B (%)	Unit weight (kg/m <sup>3</sup> )					AEWR (%)	Compressive strength (MPa)		Elastic modulus (GPa)	Modulus of rupture (MPa)
		W	C	BFS	S	G		1 day	28 days		
27.5	60	163	237	356	671	916	0.7	56.7	65.9	32.6	6.50

concrete product and to develop high strength at an early age. The temperature history of steam curing is shown in Fig. 2.

The compressive strength tests were carried out using five cylindrical specimens for each variable and curing ages according to ASTM C39 (ASTM 2014). The concrete cylinders were steam cured with the temperature history of Fig. 2, and then cured in water until the test day. A uniaxial load was applied at the monotonic rate of 0.1 mm/min using a universal testing machine with the maximum capacity of 250 ton. The compressive strength test results are shown in Fig. 3. The smaller the W/B ratios, the denser the concrete structure, resulting in the increased compressive strength. However, the W/B ratio of 25% was excluded from the optimized mix proportion, because the target slump is difficult to achieve and a large amount of water-reducing agent should be used. As the content of the blast furnace slag increased (at  $\leq 60\%$ ), the early-age strength as well as the long-term strength of concrete increased. The long-term strength improvement due to OPC replacement of the blast furnace slag is a general result, but early-age strength improvement is not common. The reason why specimens including BFS showed higher strengths in the present work, even at early ages, could be explained by the fact that the proportion of C-S-H and the apparent activation energy of concrete increased by increasing the BFS replacement ratio. According to a previous study performed by Barnett *et al.* (2006), under standard curing conditions, mortar including BFS exhibited slower strength development than that of mortar composed of Portland cement only, whereas under higher curing temperatures, the strength gain was much faster and the enhancement of early age strength was much more significant for cements with higher BFS replacement ratios, apparently owing to the greater activation energy. Based on the results of the mixing and the compressive strength test, the mix proportion of 27.5BS60, of which the water to binder ratio is 27.5% and the blast furnace slag replacement ratio is 60%, was selected as the optimized mix proportion. The optimized mix proportion was able to maximally substitute the industrial by-products, and the target compressive strengths at the ages of 1-day and 28 days were stably satisfied.

### 3.1.2 Mechanical properties of concrete

The derived mechanical properties including the compressive strength, modulus of elasticity, and modulus of rupture of the optimized mix proportion are presented in Table 2. The modulus of elasticity was calculated according to ASTM C469 (ASTM 2014), using the secant modulus for the strength corresponding to 40% of the maximum compressive strength in the stress-strain relationship obtained by a compression test of concrete. Cylindrical specimens of 100 mm in diameter and 200 mm long were

used and the linear variable differential transformer (LVDT) was attached to each specimen in order to measure the displacement, then the strain was calculated and reflected in the following equation given in ASTM C469 (ASTM 2014)

$$E = \frac{(f_2 - f_1)}{\varepsilon_2 - 0.00005} \quad (1)$$

where  $E$  is the chord modulus of elasticity,  $f_2$  is the stress corresponding to 40% of the ultimate load of the concrete,  $f_1$  is the stress corresponding to a longitudinal strain of 50 millionths, and  $\varepsilon_2$  is the longitudinal strain produced by stress  $f_2$ . The prediction value of elastic modulus was 34.3 GPa using the following equation for elastic modulus of normal-density concrete with normal-weight, provided by the Korea Structural Concrete Design Code (KCI 2012).

$$E_c = 8,500 \cdot \sqrt[3]{f_{cu}} \quad (2)$$

where  $E_c$  is the secant modulus of elasticity of concrete and  $f_{cu}$  is the average compressive strength of concrete at 28 days after curing. The measured elastic modulus of the optimized mixture was slightly lower than that of the predicted value.

In order to measure the modulus of rupture, the specimen with a section of 100 mm × 100 mm and length of 400 mm was manufactured and a four-point flexural test was performed based on ASTM C1609 (ASTM 2012). The flexural strength was calculated using the equation  $PL/bh^2$ , where  $P$  is the applied load,  $L$  is the clear span length, 300 mm,  $b$  is the beam width, 100 mm, and  $h$  is the beam height, 100 mm. The prediction value of modulus of rupture was 4.88 MPa according to the following equation for normal-density concrete with normal-weight, provided by the Korea Structural Concrete Design Code (KCI 2012).

$$f_r = 0.63\sqrt{f_{ck}} \quad (3)$$

where  $f_r$  is the rupture strength of concrete, and  $f_{ck}$  is the specified compressive strength of concrete. The measured modulus of rupture showed a larger value when compared with the prediction equation.

### 3.1.3 Durability of concrete

The repeated freezing and thawing test, carbonation resistance test, and permeability test were all performed in order to evaluate the durability of the optimized mixture. Repeated freezing and thawing causes cover spalling, surface scaling, and internal cracking of the concrete. The repeated freezing and thawing test was performed according to KS F2584 (KS 2013) and ASTM C666 (ASTM 2015). Repeated freezing (4 to -18 °C) and thawing (-18 to 4 °C) cycles were applied to the 100 × 100 × 400 mm prismatic beam specimens. The fundamental transverse frequency, in order to determine the relative dynamic modulus of elasticity, as well as the mass of each specimen, were measured every 30 freeze-thaw cycles. The mass changes were also measured so as to observe the surface deterioration during these same cycles. Fig. 4 shows the relative dynamic elastic modulus and ratio of mass change with varying cycles of freezing and thawing. The OPC, a mixture with no mineral admixtures, and the BS60, an

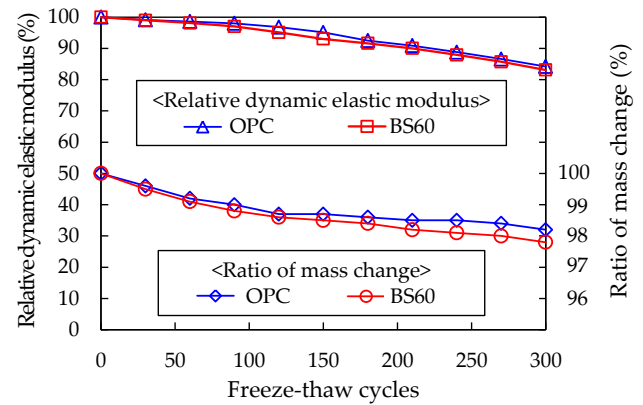


Fig. 4 Result of rapid freezing and thawing resistance test

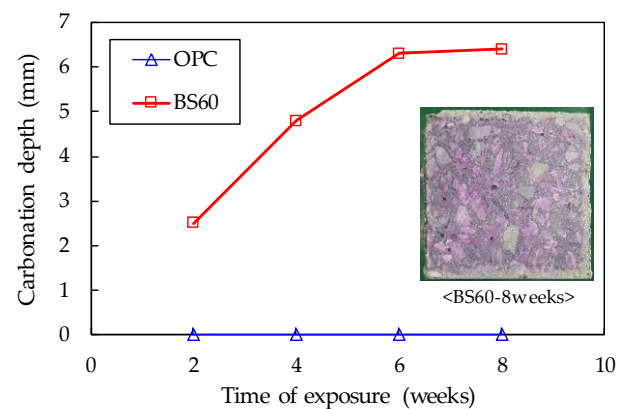


Fig. 5 Result of accelerated carbonation test

optimized mixture with 60% replacement of blast furnace slag, exhibited 84.2% and 83.1% relative dynamic elastic moduli during 300 cycles of the rapid freezing and thawing test, respectively, and all showed a durability index over 80. The results of the mass change ratio were also similar. These results indicate that the optimized mixture has a good compressive strength and a tight matrix structure that develops sufficient tensile strength so as to resist the occurrence of expansion force during the freezing of water in the capillary pores.

The carbonation resistance was investigated by an accelerated carbonation test based on KS F2584 (KS 2010). The carbonation of concrete reduces the natural alkalinity of the concrete, resulting in a reduction of concrete mechanical properties as well as the corrosion of steel rebars in the concrete. The prismatic beam specimens of 100 × 100 × 400 mm were fabricated, and four surfaces were coated using polyurethane on only the two opposite side surfaces that are uniformly exposed to the carbon dioxide. The specimens were then placed in the accelerated carbonation chamber, which maintains a CO<sub>2</sub> concentration of 5 ± 0.2%, and exposed to the carbonation environment for eight weeks. Every two weeks during this eight-week period, each 60 mm-thick sample was cut, thereafter carbonation depth was measured after a 1% phenolphthalein solution was sprayed on a cut surface of the sample. The carbonation resistance test results are shown in Fig. 5. As expected, the carbonation speed of the optimized mixture with a high

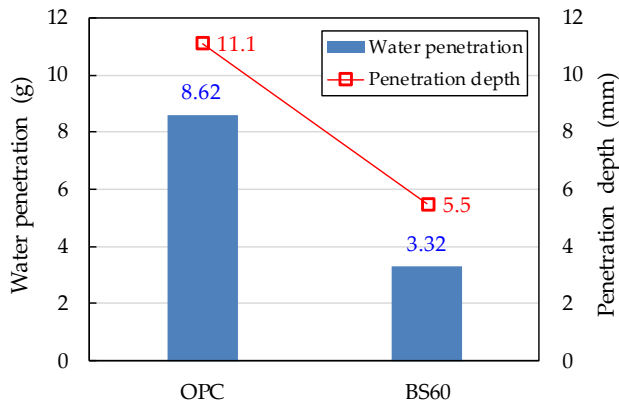


Fig. 6 Result of penetration test

Table 3 Mechanical properties of strand (KS 2008; Yang *et al.* 2016)

Item	Breaking strength (kN)	Yield (0.2% proof) strength (kN)	Elongation (%)	Modulus of elasticity (GPa)	Relaxation (%)
<sup>a)</sup> 1860 MPa Spec.	261.0	222.0	3.5	185.0~205.0	2.5
<sup>b)</sup> 2400 MPa Spec.	333.0	283.0	3.5	185.0~205.0	2.5
<sup>c)</sup> 2400 MPa Result	347.5	321.7	7.5	198.7	0.8

[Note] <sup>a)</sup> and <sup>b)</sup> = minimum properties of 1860 MPa and 2400 MPa prestressing steel strands specified in KS D7002 (KS 2018), respectively, and <sup>c)</sup> = mechanical properties of a 2400 MPa strand sample used in this research.

volume of blast furnace slag was very fast compared to that of the OPC, due to the high consumption of calcium hydroxide by the pozzolanic reaction in BS60. The average carbonation coefficient,  $C$  (mm/ $\sqrt{\text{day}}$ ), of the BS60 specimen was calculated to be 0.851 mm/ $\sqrt{\text{day}}$  using the following equation (Gruyaert *et al.* 2013, Borges *et al.* 2010)

$$x = x_0 + C \cdot \sqrt{t} \quad (4)$$

where  $x$  is the depth of carbonation (mm),  $t$  is the exposure time (day), and  $x_0$  is the initial carbonation (which is usually small or zero). The service life of the structure, which uses the optimized mixture and minimum concrete cover of 40 mm, was also calculated using the following equation (Shin *et al.* 2016)

$$\frac{C_{acc}}{C_{air}} = \sqrt{\frac{(CO_2)_{acc}}{(CO_2)_{air}}} \quad (5)$$

where  $C_{acc}$  and  $C_{air}$  are the average carbonation coefficients of accelerated tests and ambient air, respectively, and  $(CO_2)_{acc}$  and  $(CO_2)_{air}$  are the  $CO_2$  concentration in accelerated tests and ambient air, respectively. If the  $(CO_2)_{acc}$  is conservatively assumed to be 0.3%, the service life was calculated as 101 years. It is noted that this 100-year service life of the optimized mixture can be secured if quality control for the concrete cover of 40 mm is guaranteed, even though the carbonation progress of the optimized mixture is faster than that of the OPC.

The penetration tests were performed according to KS

F4042 (KS 2012). The side of the dried cylinder specimen of 100 mm in diameter was waterproofed with paraffin or epoxy, and then a water pressure of 5 N/cm<sup>2</sup> was applied to the top surface of the specimen for 24 hours. Prior to and after applying the hydraulic pressure, the weight difference ( $W_2 - W_4$ ) of the specimen was calculated in order to evaluate the amount of penetration, and the penetration depth was measured after the splitting of the specimen. As shown in Fig. 6, the amount of penetration and the penetration depth of the optimized mixture were decreased by 61.5% and 50.5%, respectively, compared to OPC. This means that the matrix pore structure became dense due to the high amount of replacement with blast furnace slag.

### 3.2 2,400MPa prestressing strand

#### 3.2.1 Mechanical properties of the prestressing strand

The 2,400 MPa prestressing strand with a tensile strength, which was increased by about 28% from the 1,860 MPa conventional prestressing strand, was developed in Korea and reflected in the Korean Standard (Kim *et al.* 2013, 2016, KS 2018, Yang *et al.* 2016, 2018). If this 2,400MPa prestressing strand is used, it is possible to design PSC girders in an economical manner by reducing the number of the strands and anchorages, and by reducing the cross-sectional areas and weights of the PSC girders, and it is also possible to make eco-friendly design with low  $CO_2$  emission by reducing the amount of concrete and strands. Since the 2,400MPa prestressing strand is reflected in KS, it has been applied in various fields, such as concrete bridges, prestressed ground anchors, LPG/LNG storage tanks, and so on in Korea, and its range of applications continues to expand.

The minimum properties of the 1,860 MPa and 2,400 MPa prestressing steel strands specified in KS D7002, and mechanical properties of the 2,400 MPa strand sample used in this research were presented in Table 3 (KS 2018, Yang *et al.* 2016). The specified values of the tensile and yield strengths for 2,400 MPa strand are increased by about 28%, and the other minimum properties of elongation, elastic modulus, and relaxation for the 2,400 MPa strand remain same as those for the 1,860 MPa strand.

#### 3.2.2 Transfer length of prestressing strand

The transfer length is one of the most important properties influencing the structural design and performance of the pre-tensioned prestressed concrete beams. The transfer length varies depending on a variety of factors such as the diameter of the strand, tensile strength, concrete strength, and the detensioning method used. Among them, the stress of strands is also one of the most influential factors. The effect of the increased prestressed force of 2,400 MPa strand on the transfer length should be evaluated, for this reason, experiments for many variables such as concrete compressive strength, steel fiber volume ratio, stirrup installation, concrete cover depth, strand cutting method, etc. have been carried out (Kim *et al.* 2016, Yang *et al.* 2016, Yang *et al.* 2018).

First, 28 pretensioned PSC beams were fabricated by using 1,860 MPa and 2,400 MPa strands according to the

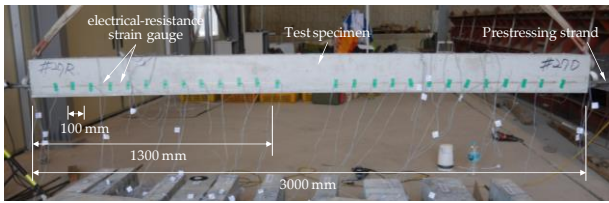


Fig. 7 Details of test specimens and attached locations of strain gauges

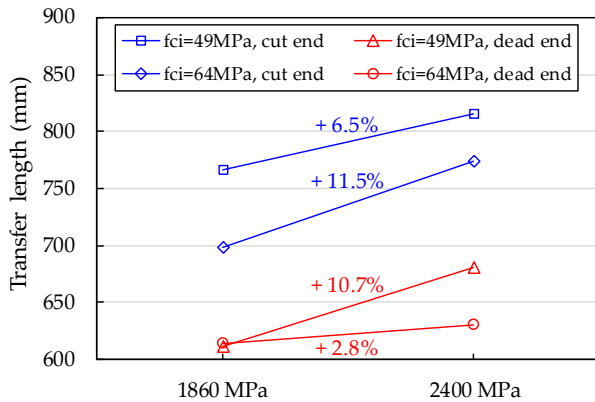


Fig. 8 Effect of prestressing force on the transfer length

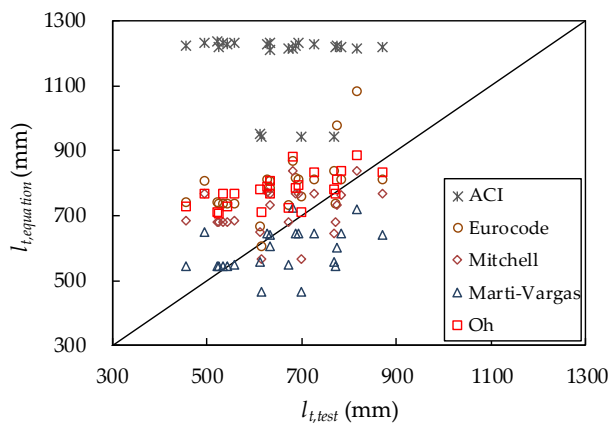


Fig. 9 Transfer length comparison between test results and equations proposed by codes and researchers

research of Kim *et al.* (2016). The concrete compressive strength at prestressing release ( $f_{ci} = 49$  and  $64$  MPa) was one of the variables. The volume fraction of the steel fibers ( $v_f = 0, 0.38, \text{ and } 0.76\%$ ) as well as the spacing ( $s_s = 50$  and  $100$  mm) and length ( $l_s = 0, 400, 800, \text{ and } 1200$  mm) of stirrup were included as variables in order to investigate their confinement effect on the transfer length. The cross-section of the fabricated concrete beams was  $115 \times 200$  mm, and the beam length was  $3,000$  mm. All of the beams had a single strand at the same location, the tensioning force of seven-wire strands was  $0.75f_{pu}$ , where  $f_{pu}$  is ultimate tensile strength of strand at  $1,860$  MPa or  $2,400$  MPa. The prestressing force was developed by the sudden release method using flame cutting at one end, and the transfer lengths were measured at each side, both the cut end and the dead end. Strain was measured by attaching an electrical-resistance strain gauge on both side surfaces of the concrete

Table 4 Design condition of two mock-up tested HPSC girders and a field applied HPSC girder

Item	Mock-up tested HPSC girder		Field applied HPSC girder
	Box-type	I-type	
Target structure	Highway bridge	Railway bridge	Railway bridge
Design concrete strength	50 MPa	60 MPa	60 MPa
Concrete strength at prestressing release	40 MPa	48 MPa	48 MPa
Tensile strength of PS strand	2400 MPa	2400 MPa	2400 MPa
Number of strands for pre-tension	2 for top flange 6 for bottom flange	6 for bottom flange	6 for bottom flange
Number of tendons for post-tension	2	2	1 for 1 <sup>st</sup> post-tension 2 for 2 <sup>nd</sup> post-tension
Tendon units for post-tension	12 hole $\times$ 2 set	19 hole $\times$ 2 set	22 hole $\times$ 1 set 10 hole $\times$ 2 set
Yield strength of rebar	400 MPa	400 MPa	400 MPa
Total length of girder	29.8 m	35 m	34.9 m
Number of segment	1 for mid-segment 2 for outside-segment	1 for mid-segment 2 for outside-segment	1 for mid-segment 4 for outside-segment
Length of mid-segment	15 m	15 m	13 m
Length of outside-segment	7.4 m	10 m	5.6 m + 5.35 m
Girder height	1.4 m	2.4 m	2.4 m
Min. web thickness	200 mm	180 mm	180 mm

beam at  $100$  mm intervals from both ends (Fig. 7).

Fig. 8 shows the effect of prestressing force on the transfer length. The  $2,400$  MPa strand higher prestressing force that was developed showed longer transfer length than the  $1,860$  MPa strand. In the case that the concrete strength was  $49$  MPa, the transfer length increased by  $6.5\%$  and  $11.5\%$ , and in the case that the concrete strength was  $64$  MPa, the transfer length increased by  $10.7\%$  and  $2.8\%$ , at the cut end and dead end, respectively. These results show that the increase of transfer length was less than half of the prestressing force increment by  $28\%$ , and this is attributed to the fact that the Hoyer effect is increased with prestressing force increase (Briere *et al.* 2013). Through these experimental results and statistical analysis, Kim *et al.* (2016) proposed a transfer length of  $2,400$  MPa prestressing strand with  $58 d_b$  at the cut end and  $55 d_b$  at the dead end, where  $d_b$  is the diameter of the strand. This proposal is larger than the approximate expression of ACI (ACI Committee 318 2014), and smaller than the AASHTO LRFD approximation (AASHTO 2017). The AASHTO LRFD design specifications require transfer lengths equal to  $60 d_b$ , and the ACI shear design guidelines require transfer lengths equal to  $50 d_b$ . The first transfer length test results for the other variables are as follows: (1) The transfer length at the cut end was larger than that at the dead end due to the impact and cracking caused by the sudden introduction of prestressing force. (2) In the cut end, the transfer length decreased with the reinforcing of steel fiber, but the

excessive inclusion of steel fiber showed a decrease in the adhesion between strand and concrete. (3) As the stirrup installed length was increased, the transfer length was decreased due to the decreasing of dynamic impact and bursting force generated by the sudden transfer of prestressing force.

The second research on the transfer length of 2,400 MPa prestressing strands was performed by Yang *et al.* (2016) in a similar way to the study of Kim *et al.* (2016). A total of 32 specimens were fabricated and their transfer lengths were measured by electric resistant strain gages. The prestressing forces were released gradually by slowly reducing the pressure in the hydraulic stressing ram. Identical prestressing stress was applied using a 2,400 MPa strand, and the main variables of the test were the concrete compressive strength ( $f_{ci} = 58 \text{ MPa}$  and  $74 \text{ MPa}$ ), concrete cover depth (40 mm, 50 mm, and 60 mm), and number of strands (1, 2, and 3). The experimental results showed that the transfer length decreased as the concrete compressive strength increased, and that the transfer length decreased as the concrete cover depth increased. In the case of a 40 mm concrete cover depth, the transfer length increased with the increase of the number of strands. This indicates that the combination of the concrete cover thickness under the strands and the distance between strands affects the transfer length. In addition, the transfer length test results were compared with prediction equations proposed by codes and researchers (ACI Committee 318, 2014, BS EN 1992-1-1, 2004, Mitchell *et al.* 1993, Marti-Vargas *et al.* 2007, Oh *et al.* 2014), as shown in Fig. 9. The transfer length model proposed by Oh *et al.* (2014), of which  $l_{t, \text{test}}/l_{t, \text{equation}}$  has the mean value of 0.83 and the coefficient of variation of 0.14, showed the most accurate and conservative results.

#### 4. Mock-up test of 30-m long HPSC girder for highway bridges

##### 4.1 Design and manufacture of girder

In order to experimentally verify the proposed HPSC girder, a 30-m long full-scale PSC box type girder was designed and fabricated utilizing low carbon materials and optimized concrete mixing with a high-volume blast furnace slag and 2,400 MPa high strength strands. The Highway Bridge Design Specification (MLIT 2005) was implemented as a structural design standard, and the DB-24 and DL-24 were employed as design criteria of the live load. The girder consisted of three parts of segment. A 15 m long mid-segment contained two and six strands for pretension in the top and bottom flanges, respectively, and the mid-segment assembled with two 7.5 m long outside-segments by two post-tensioning tendons contained twelve strands each (Fig. 10). The pre-tensioned strands were placed in a straight line on the mid-segment, on the other hand, the post-tensioned strands had a parabolic drape and were arranged uniformly on the hole length of girder. The girder had a height of 1.4 m and width of 0.8 m and had a hollow cross-section at the center with web and flange thicknesses of 200 mm. The design compressive strength of concrete was 50 MPa and the SD400 steel rebars of which

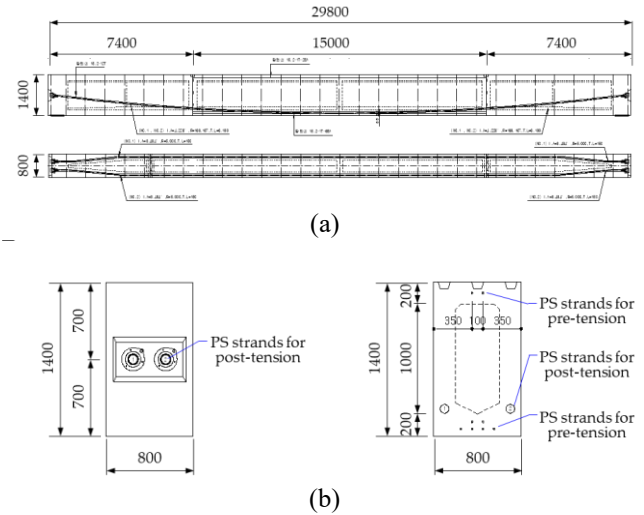


Fig. 10 Geometry of 30 m long mock-up test girder (unit: mm); (a) front view and top view, (b) cross-section at the end and center of girder



Fig. 11 Structural test and measurement of displacement for 30 m long HPSC girder

the yield strength is 400 MPa were used. The dimensions and design conditions of the tested HPSC girder are shown in Fig. 10 and Table 4, respectively.

The fabrication procedure of the tested HPSC girder was as follows: (1) The steel rebars and pre-tensioning strands were placed through the mid-segment. (2) The pre-tensioning strands of 2,400 MPa were pre-tensioned in mid-segment. (3) The pre-tensioning strands were detensioned by flame cutting when the compressive strength of concrete was over 40 MPa, after the mid-segment concrete was placed and cured by steam. (4) Two outside-segments were fabricated with a placement of rebars, sheaths, and concrete as well as steam curing of concrete. (5) After the attainment of design compressive strength of concrete the mid-segment and outside-segments were assembled by post-tensioning through the entire span. The epoxy was applied to the connections between segments before the post-tensioning in order to fill any unnecessary void. The load of 266 kN and  $0.94f_y$  for each pre-tensioning strand was applied and the load of 3,150 kN and  $0.93f_y$  for each post-tensioning tendon was applied. The lateral displacement of the combined HPSC girder by post-tensioning at the center of the mid-

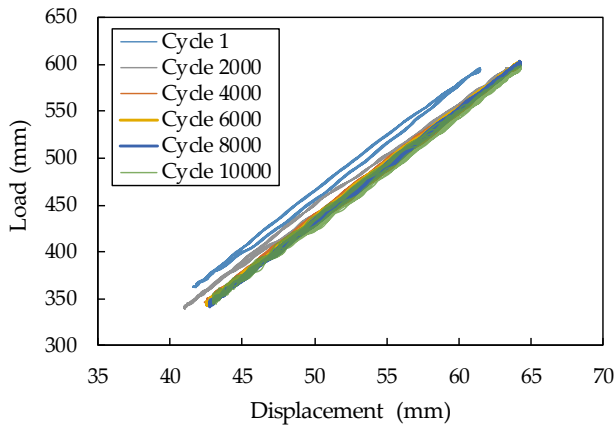


Fig. 12 Load-displacement hysteresis curve by cyclic loading at the center of 30 m long HPSC girder

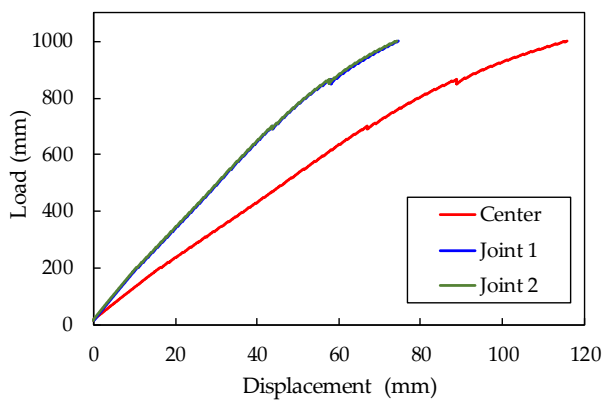


Fig. 13 Load-displacement curve by static loading at the center and joint of 30 m long HPSC girder

segment was measured at 1.63 mm. This unexpected lateral displacement may have been generated by fabrication errors at the connections between segments, and is much lower than the standard requirement for precast beams (BSI 2004), which is 0.3% of the girder length (89.4 mm for a 29.8 m long girder).

When the pre-tensioning strands were detensioned, the transfer length was measured in order to investigate the effect of girder size on the transfer length. The transfer length was measured using electric resistance strain gages attached to two bottom longitudinal rebars near the pre-tensioning strands, and the detailed process and result can be found in Yang *et al.*'s paper (2018). From the test, the average values of measured transfer length were 569 mm and 519 mm, which correspond to  $37.4d_b$  and  $34.1d_b$  at the cut end and dead end, respectively. The transfer lengths were much lower than those researched by Kim *et al.* (2016) and Yang *et al.* (2016) with small specimens. This indicates that the transfer length of the PSC beams obviously decreased with an increase in beam size.

#### 4.2 Structural test of girder

Cyclic loading and static loading tests were performed using the 30-m long HPSC girder as shown in Fig. 11. The clear span length between supports was 29.0-m, and a point

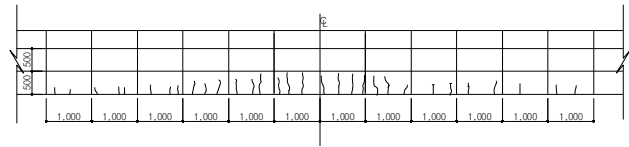


Fig. 14 Crack patterns of 30 m long HPSC girder when static loading of 1000 kN (unit: mm)

load was applied at the center of girder using an actuator with the maximum capacity of 1,000 kN. The displacement in the vertical direction was measured during the cyclic and static loading test at the center of girder and at the joints between mid-segment and outside segment.

First, ten thousand bending cyclic loads with frequency of 0.5 Hz were applied in order to evaluate the fatigue performance and stiffness degradation of the tested HPSC girder. The range of cyclic loads was from 345 kN, correspond to the service dead load, to 605 kN, correspond to the service live and dead load. Fig. 12 illustrates the plotted hysteresis curves of the measured load-displacement. As shown in Fig. 12, the identical load-displacement slope was observed, this indicate that the stiffness of HPSC girder was maintained without critical damage during service loading. Cracks were not observed visually during the cyclic loading test, not even around the segments joints. Second, the static loading test of the 30-m long HPSC girder was performed. The quasi-static load up to 1,000 kN was applied because the capacity of the dynamic actuator was limited. The measured load-displacement curves at the center and joint were plotted in Fig. 13. Cracking was first observed at the center of the girder when the loading force reached approximately 700 kN. From that point on, the crack propagation was monitored, and the obtained crack patterns are illustrated in Fig. 14. These results indicate that despite the different materials and structural system, the performance of the tested HPSC girder is similar to that of the conventional, cast-in-place 1,860 MPa monolithic post-tensioned prestressed concrete girder (Han *et al.* 2003, Yim *et al.* 2018).

## 5. Mock-up test of 35-m long girder for railway bridges

### 5.1 Design and manufacture of girder

A 35 m long full-scale I-type HPSC girder was designed and fabricated using low carbon materials, optimized concrete mixing with a high-volume blast furnace slag, and 2,400 MPa high strength strands (Yim *et al.* 2018). The Railway Design Code (MLIT 2015) was implemented as a structural design standard. The girder consisted of a 15-m long mid-segment and two 10-m long outside-segments. The cross-section of the girder was 1,000 mm  $\times$  2,400 mm, and the girder manufactured by same procedures as the 30-m long HPSC girder. The reinforced concrete slab was fabricated after the completion of the HPSC girder. The depth and width were 280 mm and 2,000 mm, and the design strengths of the concrete and rebars were 27 MPa

and 400 MPa, respectively. The details of the tested girder are described in Table 4.

When the mid-segment was manufactured, the transfer length was measured in order to investigate the effect of girder size on the transfer length by the same method as the mid-segment of 30-m long HPSC girder (Yang *et al.* 2018). The average values of measured transfer length were 291 mm and 298 mm, which correspond to  $19.1d_b$  and  $19.6d_b$  at the cut end and dead end respectively. These transfer lengths were much lower than the results of Kim *et al.* (2016) and Yang *et al.* (2016) with small specimens, even lower than those of 30-m long HPSC girder. This indicates that the girder size has a great influence on the transfer length, and the ACI's simple recommendation (ACI Committee 318 2014) for transfer length,  $50d_b$ , can be used conservatively for 2,400 MPa prestressing steel strands.

## 5.2 Structural test of girder

The fatigue test and ultimate load test for the 35-m long HPSC girder specimen were carried out in order to verify the safe of the girder for application of railroad bridges (Yim *et al.* 2018). First, the fatigue resistance performance was verified by the cyclic loading test. The design load of 817 kN, of which design live load moment was converted to the concentrated load at center, was set to the range of variation of the minimum and maximum load for the cyclic load test of two million cycles. The test results showed the elastic behavior with negligible change in slope in the load-displacement relationship, and therefore stiffness of the test specimen was not changed under cyclic loading. In order to check the occurrence of joint fissures under cyclic loading, crack measurements were installed in the joints so as to measure the displacement with loading variation. During the test, cracks in the joints and separation of segments did not occur (Yim *et al.* 2018).

Second, the static performance was verified. The vertical deflection measured at the maximum load of 2,830 kN was 82.57 mm, which was similar to the center deflection of 82.68 mm calculated by the analytical method with an error of 0.11 mm. The static test of the HPSC girder showed analytically predicted behavior and showed that the 35-m long HPSC girder had sufficient strength and safety when the maximum load of 2,830 kN was compared with the design live load of 817 kN (Yim *et al.* 2018).

## 6. Field application of HPSC girder

A 35-m actual railway bridge girder was designed and fabricated with the goal of application to the Railroad Test Track in Sejong city, Korea. The hybrid prestressing method, a combination of pre-tension and post-tension, and low carbon materials were applied to the design. As described in Table 4, the girder was designed as a combination of five segments, had a center segment of 13 m with pre-tension and two 5.6 m + two 5.35 m outside-segments, considering land transport weight limit in Korea. The use of high strength concrete with a design strength of 60 MPa (Table 2) and 2,400 MPa high strength strand (Table 3) developed in the previous study lowered the

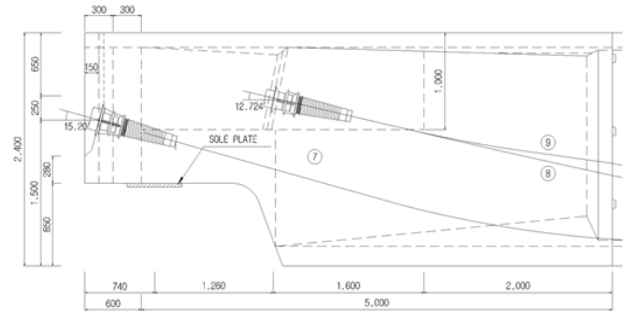


Fig. 15 Details of 1<sup>st</sup> outside segment and end cutting for field applied HPSC girder



Fig. 16 Fabrication and application procedure of HPSC girder; (a) installation of rebars for mid-segment, (b) pre-tensioning of PS strands before concrete placing, (c) completion of mid-segment through concrete placing and detensioning, (d) installation of rebars and sheath for outside-segment, (e) concrete placing and curing of outside-segment, (f) carrying segments to field, (g) combining segments by post-tensioning, (h) erecting HPSC girder, (i) completion of application

height of the 35 m long railway bridge girder to 2.4 m (existing girder: approx. 2.6 m), and minimized the web thickness, thereby, the self-weight of girder could be reduced. In addition, using 2,400MPa high strength strand instead of 1,860MPa strand, it was possible to reduce the material cost and labor cost including the number of strands and anchorage devices.

As applications of concrete bed tracks are expanded and bridge spans become longer, controlling the deflection and camber of bridges becomes increasingly important in order to secure the driving safety and serviceability of the high speed trains. For this reason, the Railway Construction Specification (MLIT 2011) specifies the camber tolerance to be  $\pm 20$  mm. The first post-tension force for assembly of segments was introduced before girder installation, and then the second post-tension force was introduced for strengthening of the girders after girder installation, slab concrete casting and curing. This sequential post-tensioning could control the camber to be less than 20 mm at the time of concrete bed installation. In addition, the step of mounting the girder on the pier is most unstable during the girder construction because of the high risk of overturn due

to the rise of the center of gravity. Accidents due to girder overturn occur most often before the connection is achieved between girders by cross beams after the mounting the girder. In order to prevent accidents, the field applied HPSC girders were end-cut, so that the center of gravity was moved downward and the resilience against girder overturn was increased (Fig. 15).

Fig. 16 shows the fabrication and application procedures of HPSC girder that can be described as follows:

(1) The reinforcing bars were installed through the mid-segment.

(2) A total of six strands of 2,400 MPa were pre-tensioned before the concrete pouring in mid-segment.

(3) Mid-segment concrete was placed and steam cured.

(4) The pre-tensioning strands were detensioned using sudden release when the compressive strength of concrete was over 70% of design strength.

(5) The reinforcing bars and sheath were installed for the 1st and 2nd outside-segments.

(6) The outside-segment concrete was placed and steam cured.

(7) All segments were carried to field after the attainment of design compressive strength of concrete.

(8) Five pieces of segment were combined by epoxy and 1st post-tensioning of a 22 hole-tendon.

(9) The combined girders were erected to girder supports of piers.

(10) Two 10 hole-tendons were post-tensioned and grouted after the placing and curing of slab concrete.

Totally five HPSC girders were applied and the field application of HPSC girders was successfully completed without any problems. The entire bridge will be completed by the end of 2018.

## 7. Conclusions

A new prestressed concrete girder utilizing low carbon materials and hybrid prestressing concept was developed. The following conclusions were drawn through material, structural verification, and field application during the development process:

(1) The optimized high strength concrete mixture replacing blast furnace slag with 60% for PSC girder was obtained, and its target compressive strengths at the age of 1-day and 28 days, 48 MPa and 60 MPa, respectively, were stably satisfied.

(2) The optimized mixture showed equal or superior freezing and thawing resistance and permeability resistance compared with existing concrete mixture. Its carbonation resistance was worse, but it could secure an evaluated 100-year service life.

(3) The transfer length of 2,400 MPa prestressing strand was proposed so that ACI's simple recommendation for transfer length,  $50 d_b$ , could be used conservatively.

(4) The concept of HPSC girder is an efficient concept that combines the advantages of pre-tension and post-tension.

(5) The 30-m long HPSC girder for highway bridges and 35-m long HPSC girder for railway bridges were

manufactured and those structural performances were verified as having sufficient strength and safety.

(6) A 35-m HPSC girder was successfully applied to Railroad Test Track in Osong, and its widespread application is expected.

## Acknowledgements

This research was supported by a grant (13SCIPA01) from Smart Civil Infrastructure Research Program funded by Ministry of Land, Infrastructure and Transport (MOLIT) of Korea government and Korea Agency for Infrastructure Technology Advancement (KAIA).

## References

- AASHTO (2017), *AASHTO LRFD Bridge Design Specifications*, American Association of State Highway and Transportation Officials, Washington, D.C., U.S.A.
- ACI Committee 318 (2014), *Building Code Requirements for Structural Concrete (ACI 318-14) and Commentary*, American Concrete Institute, Farmington Hills, Michigan, U.S.A.
- ASTM C1609/C1609 M (2012), *Standard Test Method for Flexural Performance of Fiber-reinforced Concrete (Using Beam with Third-Point Loading)*, ASTM International, West Conshohocken, Pennsylvania, U.S.A.
- ASTM C39/39M (2014), *Standard Test Method for Compressive Strength of Cylindrical Concrete Specimens*, ASTM International, West Conshohocken, Pennsylvania, U.S.A.
- ASTM C469/469M (2014), *Standard Test Method for Static Modulus of Elasticity and Poisson's Ratio of Concrete in Compression*, ASTM International, West Conshohocken, Pennsylvania, U.S.A.
- ASTM C666/C666M (2015), *Standard Test Method for Resistance of Concrete to Rapid Freezing and Thawing*, ASTM International, West Conshohocken, Pennsylvania, U.S.A.
- Barnett, S.J., Soutsos, M.N., Millard, S.G. and Bungey, J.H. (2006), "Strength development of mortars containing ground granulated blast-furnace slag: Effect of curing temperature and determination of apparent activation energies", *Cement Concrete Res.*, **36**(3), 434-440.
- Borges, P.H.R., Costa, J.O., Milestone, N.B., Lynsdale, C.J. and Streatfield, R.E. (2010), "Carbonation of CH and CeSeH in composite cement pastes containing high amounts of BFS", *Cement Concrete Res.*, **40**, 284-292.
- Briere, V., Harries, K.A., Kasanc, J. and Hagerd, C. (2013), "Dilation behavior of seven-wire prestressing strand-the Hoyer effect", *Constr. Build. Mater.*, **40**, 650-658.
- British Standards Institution (2004), *Eurocode 2: Design of Concrete Structures: Part 1-1: General Rules and Rules for Buildings*, British Standards Institution.
- CEN (2004), *EN 1992-1-2 Eurocode 2: Design of Concrete Structures. Part 1-2: General Rules-Structural Fire Design Comité Européen de Normalisation*, Brussels, Belgium.
- Gruyaert, E., Heede, P.V. and Belie, N.D. (2013), "Carbonation of slag concrete: Effect of the cement replacement level and curing on the carbonation coefficient effect of carbonation on the pore structure", *Cement Concrete Compos.*, **35**(1), 39-48.
- Hamilton, H.R. and Brenkus, N.R. (2013), *Long Spans with Transportable Precast Prestressed Girders*, University of Florida (Sponsored by Florida Department of Transportation), Michigan, U.S.A.
- Han, M.Y., Hwang, E.S. and Lee, C. (2003), "Prestressed concrete

- girder with multistage prestressing concept”, *ACI Struct. J.*, **100**(6), 723-731.
- Jeon, J.K., Moon, H.Y., Ann, K.Y., Kim, H.S. and Kim, Y.B. (2006), “Effect of ground granulated blast furnace slag, pulverized fuel ash, silica fume on sulfuric acid corrosion resistance of cement matrix”, *Int. J. Concrete Struct. Mater.*, **18**(2E), 97-102.
- KCI (2012), *Korea Structural Concrete Design Code*, Korea Concrete Institute, Seoul, Korea.
- Kim, J.K., Seong, T.R., Jang, K.P. and Kwon, S.H. (2013), “Tensile behavior of new 2,200 MPa and 2,400 MPa strands according to various types of mono anchorage”, *Struct. Eng. Mech.*, **47**(3), 383-399.
- Kim, J.K., Yang, J.M. and Yim, H.J. (2016), “Experimental evaluation of transfer length in pretensioned concrete beams using 2,400-MPa prestressed strands”, *J. Struct. Eng.*, **142**(11), 04016088.
- KS D7002 (2018), *Uncoated Stress-relieved Steel Wires and Strands for Prestressed Concrete*, Korean Standards Association, Seoul, Korea.
- KS F2456 (2013), *Standard Test Method for Resistance of Concrete to Rapid Freezing and Thawing*, Korean Standards Association, Seoul, Korea.
- KS F2584 (2010), *Standard Test Method for Accelerated Carbonation of Concrete*, Korean Standards Association, Seoul, Korea.
- KS F4042 (2012), *Polymer Modified Cement Mortar for Maintenance in Concrete Structure*, Korean Standards Association, Seoul, Korea.
- Mahmoud, E., Ibrahim, A., El-Chabib, H. and Patibandla, V.C. (2013), “Self-consolidating concrete incorporating high volume of fly ash, slag, and recycled asphalt pavement”, *Int. J. Concrete Struct. Mater.*, **7**(2), 155-163.
- Marti-Vargas, J.R., Arbelaez, C.A., Serna, P., Navarro-Gregori, J. and Pallares-Rubio, L. (2007), “Analytical model for transfer length prediction of 13 mm prestressing strand”, *Struct. Eng. Mech.*, **26**(2), 211-229.
- Menéndez, G.V.B.B., Bonavetti, V. and Irassar, E.F. (2003). “Strength development of ternary blended cement with limestone filler and blast-furnace slag”, *Cement Concrete Compos.*, **25**(1), 61-67.
- Ministry of Land, Infrastructure and Transportation (MLIT) (2005), *Highway Bridge Design Specification*, Ministry of Land, Infrastructure and Transportation, Korea.
- Ministry of Land, Infrastructure and Transportation (MLIT) (2011), *Railway Construction Specification*, Ministry of Land, Infrastructure and Transportation, Korea.
- Ministry of Land, Infrastructure and Transportation (MLIT) (2015), *Railway Design Code*, Ministry of Land, Infrastructure and Transportation, Korea.
- Mitchell, D., Cook, W.D., Khan, A.A. and Tham, T. (1993), “Influence of high strength concrete on transfer and development length of pretensioning strand”, *PCI J.*, **38**(3), 52-66.
- Oh, B.H., Lim, S.N., Lee, M.K. and Yoo, S.W. (2014), “Analysis and prediction of transfer length in pretensioned, prestressed concrete members”, *ACI Struct. J.*, **111**(3), 549-560.
- Shin H.O., Yang, J.M., Yoon, Y.S. and Mitchell, D. (2016), “Mix design of concrete for prestressed concrete sleepers using blast furnace slag and steel fibers”, *Cement Concrete Compos.*, **74**, 39-53.
- Yang, J.M., Kim, J.K. and Yoo, D.Y. (2018), “Transfer length in full-scale pretensioned concrete beams with 1.4 m and 2.4 m section depths”, *Eng. Struct.*, **171**, 433-444.
- Yang, J.M., Yim, H.J. and Kim, J.K. (2016), “Transfer length of 2,400 MPa seven-wire 15.2 mm steel strands in high-strength pretensioned prestressed concrete beam”, *Smart Struct. Syst.*, **17**(4), 577-591.
- Yang, J.M., Yoo, D.Y., Kim, Y.C. and Yoon, Y.S. (2017), “Mechanical properties of steam cured high-strength steel fiber-reinforced concrete with high-volume blast furnace slag”, *Int. J. Concrete Struct. Mater.*, **11**(2), 391-401.
- Yim, H.J., Yang, J.M. and Kim, J.K. (2018), “Improved prestressed concrete girder with hybrid segments system”, *Struct. Eng. Mech.*, **65**(2), 183-190.

CC